A&A 556, A103 (2013)
DOI: 10.1051/0004-6361/201321919

Astronomy & Astrophysics

Hyperfine structure investigations of atomic niobium with optogalvanic and laser-induced fluorescence spectroscopy in the near-infrared wavelength range

Gö. Başar[1], Gü. Başar[2], I. K. Öztürk[1], A. Er[1], F. Güzelçimen[1], and S. Kröger[3]

[1] Istanbul University, Faculty of Science, Physics Department, 34134 Vezneciler, Istanbul, Turkey
e-mail: gbasar@istanbul.edu.tr
[2] Istanbul Technical University, Faculty of Science and Letters, Physics Engineering Department, 34469 Maslak, Istanbul, Turkey
[3] Hochschule für Technik und Wirtschaft Berlin, Fachbereich 1, Wilhelminenhofstr. 75A, 12459 Berlin, Germany
e-mail: sophie.kroeger@htw-berlin.de

Received 19 May 2013 / Accepted 29 June 2013

ABSTRACT

Aims. The aim of this work is to increase the amount of hyperfine structure data of atomic niobium (Nb I), which is needed for astrophysicists for the detailed analysis of new stellar spectra. Particular emphasis was placed on the investigation of energy levels with unknown hyperfine structure constants.
Methods. The hyperfine structure in the spectrum of Nb I was studied using laser-induced fluorescence spectroscopy and laser optogalvanic spectroscopy with a tuneable single-mode cw Ti:Sa laser in the wavelength range from 750 nm to 865 nm. The Nb atoms were produced and excited in a liquid-nitrogen-cooled hollow-cathode plasma.
Results. We measured and analysed 81 spectral lines, 19 of which are not previously known from the literature. In total, the magnetic dipole hyperfine structure constants A were determined for 28 energy levels of even and 53 energy levels of odd parity. The electric quadrupole hyperfine structure constants B were only determined in a few cases, when the spectra were clearly resolved and/or when a level was found from several transitions. The magnetic dipole hyperfine structure constants A of 13 even and 11 odd levels as well as the electric quadrupole hyperfine structure constants B of 13 even and 17 odd levels are presented for the first time. For the other levels, improved values of hyperfine structure constants are given.
Conclusions. The hyperfine structure can have a significant effect on stellar absorption line profiles, and the corresponding abundances can be substantially overestimated if these effects are not taken into account. Therefore, a detailed consideration of the hyperfine structure is important for stellar abundance determinations. The present work substantially increases the knowledge of hyperfine structure of Nb, which plays an important role in investigating the nucleosynthesis of heavy elements.

Key words. atomic data – line: profiles – techniques: spectroscopic – methods: laboratory

1. Introduction

We here continue our earlier systematic investigations of the spectrum of Nb I (Kröger & Bouzed 2003; Kröger et al. 2004, 2007, 2010; Başar et al. 2008; Er et al. 2011). Our purpose is to supplement hyperfine structure (hfs) data for this element, in particular, to fill gaps for all energy levels of even parity with unknown hyperfine structure (hfs) constants.

Niobium[1] (Nb) is the third element of 4d shell transition elements and belongs to the very few elements with only one stable isotope. The astrophysical interest of Nb hfs data was already extensively discussed in Kröger et al. (2010). A lot of work has already been done over the past 35 years to investigate the hfs of Nb using various spectroscopic methods. For the low-lying energy levels hfs constants have been determined with very high accuracy using atomic-beam magnetic-resonance method by Büttgenbach et al. (1975). Other high-resolution measurements have been made by Fraenkel et al. (1988) using laser and radio-frequency spectroscopy, and by some of us (Başar et al. 2008), using Doppler-reduced saturation absorption spectroscopy. Doppler-limited measurements of hfs constants have been made using Fourier transform spectroscopy (Kröger et al. 2010; Er et al. 2011) and Doppler-limited laser spectroscopic methods (Singh & Rao 1989; Singh et al. 1992; Bouzed et al. 2003; Kröger 2007). In addition to the experimental investigations, a theoretical analysis of hfs of atomic Nb has been performed by Büttgenbach & Dicke (1975), Kröger & Bouzed (2003), and Kröger et al. (2007).

Despite all this effort, for many energy levels the hfs constants are still unknown, some of them lying relatively low, i.e. lower than 25 000 cm^{-1}. Until now, the magnetic dipole hfs constants A of 57 levels of even and 136 levels of odd parity as well as the electric quadrupole hfs constants B of 32 levels of even and 30 levels of odd parity are known. In the present work, we increase the data by 24 A (13 for even and 11 for odd parity levels), filling all gaps for levels of even parity, which have had not yet known A constants. Additionally, 31 new B constants (13 for even and 18 for odd parity levels, respectively) were determined.

[1] Its name was columbium (Cb) up to the 1950s.

2. Experimental details

The Nb atoms were produced and excited in a cooled hollow-cathode plasma. The hollow-cathode lamp consists of mainly two anodes and a 20 mm long hollow cathode with a 3 mm inner diameter in which a 0.125-mm-thick niobium foil was inserted. The hollow cathode was cooled by liquid nitrogen to reduce the Doppler width. A detailed explanation of the construction of the hollow-cathode lamp is given in Messnarz & Guthöhrlein (2000). The discharge was operated at a Ne pressure of about 2 mbar and a current of 10 to 50 mA. The current was chosen depending on the signal-to-noise ratio of the spectral line. The low current is favourable to reduce the Doppler width, whereas the high current increases the signal.

A continuous wave tuneable titan-sapphire (Ti:Sa) laser (Coherent MBR-110 pumped by Coherent Verdi 18 W) was used in the wavelength range from 750 nm to 865 nm with a power of about 1.5 W. Two small parts of the laser beam were split off by a beam sampler to measure spectral properties. The first beam part was directed to a home-made temperature stabilized confocal Fabry-Perot interferometer (FPI) with a free spectral range of about 300 MHz, which was used to measure the variation of the relative frequency during the scan of the laser wavelength. The spectrum from the FPI was used to calibrate the simultaneously measured atomic spectrum. The second part of the laser beam was coupled to a wavemeter (High Finesse WS6-200), which has an accuracy for the absolute frequency of 200 MHz or 0.007 cm^{-1}. By using a couple of dielectric mirrors, the main laser beam went through the hollow-cathode lamp after passing from the backside through the hole of the large diameter mirror that has a hole in the middle (outer diameter: ∅ = 100 mm, hole diameter: ∅ = 3 mm).

The experimental setup was constructed so that both the laser optogalvanic spectroscopy (LOGS) and laser-induced fluorescence spectroscopy (LIFS) could be applied simultaneously (see Fig. 1). The laser beam was amplitude-modulated by a mechanical chopper to apply a lock-in technique that recovered the signal deduced from LOGS and LIFS.

The optogalvanic signal was produced when the wavelength of the laser was resonant with the differences of energy levels of Nb or noble gas atoms. The change of voltage was measured across a ballast resistor. A detailed explanation of the optogalvanic effect can be found in Sasso (1990).

For LIFS measurements, the large-diameter hole mirror collected the divergent fluorescence light from the hollow cathode. The fluorescence light was collimated by a lens, directed to the monochromator by two large diameter mirrors (∅ = 100 mm) and focused on the entrance slit by another lens. The monochromator (McPherson 607, 0.67 m focal length and a (120 mm × 140 mm) large grating with 1200 lines/mm; photomultiplier PM R928 from Hamamatsu) was used as a fixed wavelength filter to measure only the fluorescence light arising from transition including one of the energy levels, which are involved in the transition excited by the laser. A detailed explanation of the LIFS method can be found in Shamim et al. (2011).

The two signals from LOGS and LIFS could be observed simultaneously. By scanning the laser wavelength, the hfs of the investigated spectral lines could be detected. For some lines, the signal-to noise ratio was better using LOGS than LIFS. For other lines, it was the opposite. For each line, the best method was chosen. For LIFS measurements, different fluorescence transitions were tried and the best was picked up.

In LOGS measurements, some lines were overlapping within their hfs pattern with other Nb or Ne lines. For these lines,

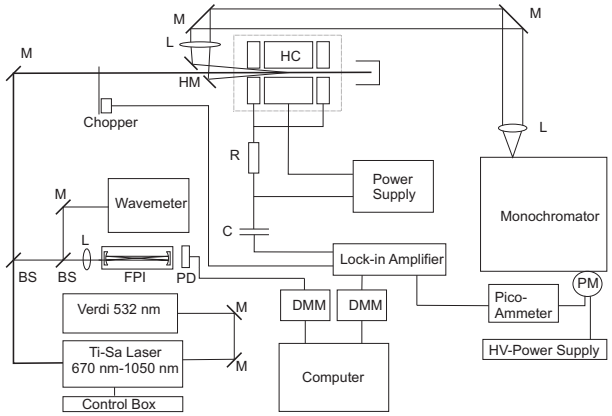

Fig. 1. Schematic overview of the experimental setup used for laser optogalvanic spectroscopy and laser-induced fluorescence spectroscopy; M: mirror, L: lens, BS: beam sampler, FPI: Fabry-Perot interferometer, R: resistor, C: capacitor, HC: hollow-cathode lamp, DMM: digital multimeter, PD: photodiode, HM: hole mirror, PM: photomultiplier, HV: high-voltage power supply.

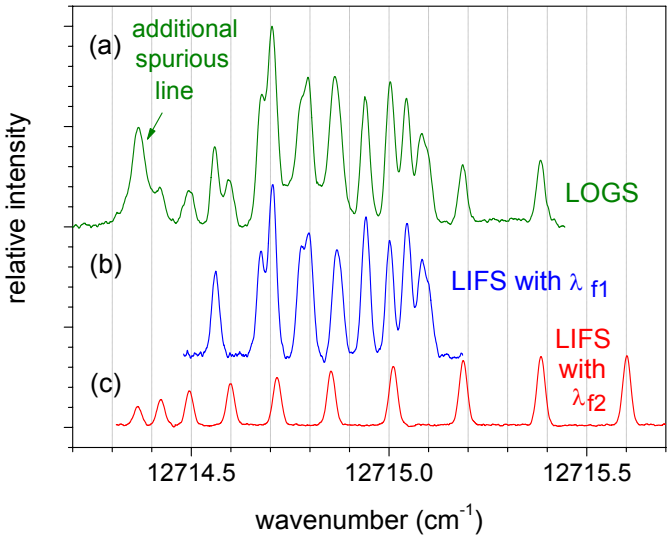

Fig. 2. Example for blended lines: **a)** Spectrum recorded by LOGS at around 12 715 cm^{-1} showing the overlap of two Nb lines as well as another spurious line. **b)** Spectrum recorded by LIFS with fluorescence λ_f = 532.15 nm: transition from 14 899.26 cm^{-1}, J = 5/2 ⟶ 27 614.10 cm^{-1}, J = 5/2 at λ_{air} = 786.266 nm or σ_{vac} = 12 714.84 cm^{-1}. **c)** Spectrum recorded by LIFS with fluorescence λ_f = 581.94 nm: transition from 17 476.22 cm^{-1}, J = 11/2 ⟶ 30 191.25 cm^{-1}, J = 13/2 at λ_{air} = 786.255 nm or σ_{vac} = 12 715.03 cm^{-1}.

LIFS was very convenient and offered the possibility to separate the lines by using different fluorescence channels. An example for overlapping hfs patterns is given in Fig. 2. The spectrum recorded with LOGS is compared with two spectra measured with LIFS using two different fluorescence wavelength. Only by using LIFS with two different fluorescence wavelengths was it possible to separate the lines.

3. Selection of lines

As mentioned above, the aim of the present work was to fill up gaps in the knowledge of hfs constants A, especially for

levels of even parity. The classification program Class_lw from Windholz & Guthöhrlein (2003) was used to search for transitions involving levels with unknown A constants. A comprehensive list of experimental wavelengths and classifications for Nb I and II, as well as a list of corresponding energy levels is given by Humphreys & Meggers (1945) (nearly 70 years, old but still very useful). This list provides the basis for the classification program, supplemented by new energy levels from more recent references (Kröger et al. 2004, 2007), (resulting in the same list as the current state of the level list, given in the NIST atomic spectra database (NIST 2013)). The program additionally contains information about magnetic dipole and electric quadrupole hfs constants A and B, if available. Using the Ritz combination principle and taking into account the selection rule for electric dipole transitions ($\Delta J = 0, \pm 1$; $J = 0 \nleftrightarrow 0$), the program calculates all possible transitions to and from a chosen energy level. The program does not consider transition probabilities and of course provides much more lines than listed in the wavelength table of Humphreys & Meggers (1945). Therefore, not all transitions calculated by the Ritz combination principle could be found with our experimental conditions.

We measured and classified 81 spectral transitions (see Table 1). Sixty-two of these lines have already been listed in the wavelength tables from Humphreys & Meggers (1945), 14 without classification. The classification for these lines was deduced from the classification program Class_lw using the hfs patterns as fingerprint. Nineteen lines were not previously known from the literature.

4. Hyperfine structure analysis

The hyperfine structure (hfs) describes higher-order interactions of the nuclear moments with the magnetic and electric fields produced by the electrons at the site of the nucleus. It results in a splitting of a fine structure energy level E, (characterized by the total electronic angular momentum quantum number J), into hfs sublevels when an isotope has a nuclear spin I greater than zero. The hfs sublevels are characterized by the total angular momentum quantum number F, which can take values from $|J - I|$ to $(J + I)$. Hence, the number of hfs sublevels is equal to the minimum of $(2J + 1)$ or $(2I + 1)$. The hfs interaction energy $E_{\rm hfs}$ of a hfs sublevel is given by

$$E_{\rm hfs}(F) = A\frac{K}{2} + B\frac{3K(K+1) - 4(I(I+1)J(J+1)}{8I(2I-1)J(2J-1)}, \quad (1)$$

where A and B are the hfs constants for the magnetic dipole and electric quadrupole interaction, respectively, and

$$K = F(F+1) - I(I+1) - J(J+1).$$

The first term in Eq. (1) is caused by the magnetic dipole interaction and the second term by the electric quadrupole interaction. A and B are specific for each fine structure level. If only the magnetic dipole hfs is taken into account, the energy difference between hfs sublevels can be simply calculated by the Landé interval rule:

$$E_{\rm hfs}(F+1) - E_{\rm hfs}(F) = A\,(F+1). \quad (2)$$

The selection rule for optical transitions between hfs sublevels is given by

$$\Delta F = 0, \quad \pm 1 \quad (F = 0 \nleftrightarrow 0).$$

The relative intensity of hfs transitions is given by

$$\text{rel.int.} = (2F_u + 1)(2F_l + 1)\begin{Bmatrix} I & F_u & J_u \\ 1 & J_l & F_l \end{Bmatrix}, \quad (3)$$

where the indices u and l indicate the upper and lower level, respectively. Transitions with $\Delta J = \Delta F$ have the highest intensity.

The only stable niobium isotope ^{93}Nb has a nuclear spin of $I = 9/2$ and a large magnetic dipole moment of $\mu_I = +6.1705\,(3)\ \mu_N$ (Lederer & Shirley 1978). Therefore it is reasonable to apply Doppler-limited experimental techniques to determine the magnetic dipole hfs constants A. The comparatively small electric quadrupole moment of $Q = -0.36\,(7)$ barn (Lederer & Shirley 1978) leads to a weak deviation of the hyperfine splitting from the interval rule (see Eq. (2)), which is not always detectable in Doppler-limited spectra.

For analysing the recorded spectra, the wave number axis were linearised using the free spectral range of the FPI. The free spectral range is calibrated to 299.0010 (8) MHz, which corresponds to a relative accuracy of 3×10^{-4}%.

To obtain the hfs constants A and B, the linearised spectra were fitted using the program Fitter (Guthöhrlein 2004), which takes into consideration Eq. (1). The fit parameters were

- the centre of gravity of the total hfs;
- the A and B constants of the upper and the lower level;
- the intensities and the Gaussian and Lorentzian parts of the Voigt profile of the individual hfs components;
- two parameters to take into account height and slope of the background.

For all measured lines the observed intensity ratios of the hfs components differ from the theoretical intensity ratios given in Eq. (3). This is caused by hyperfine pumping and by the saturation effect due to the high power of the laser. This effect results in an intensity reduction and broadening of the strong hfs components and leads to an apparent intensity increase of the weak components. As a consequence, the ratio of the intensities of the components is not in accordance with the theoretical ratios. The Lorentzian contribution differs for the individual hfs components, whereas the Gaussian contribution is the same for all hfs components of a line. For this reason, the parameter for the Gaussian half width was set to the same value for all hfs components of a line, whereas the parameters for Lorentz half width and intensity may vary. To illustrate the magnitude of intensity increase of the weak components, a spectrum of a fully resolved line is shown in Fig. 3 together with the theoretical relative intensities, given as arrows. The arrows are normalised to the strongest hfs component. Intensity increases up to factors higher than 6 are measured.

Depending on the discharge current and on the wavelength, the Gaussian line width varied from 540 MHz to 820 MHz for the different lines.

As discussed above, the influence of the electric quadrupole interaction on the hfs is small. Therefore, it was possible to determine reliable values for the B constants only when a line had at least four clearly resolved individual hfs components. In these cases, the B constants were fitted as free parameters. In all other cases, the B constants were fixed to be equal to zero (except for a few unresolved lines, where A and B constants for one level were fixed equal to previously known values, see below).

All spectra with clearly resolved hfs components (as for example the line shown in Fig. 3) are fitted with individual Lorentz half widths and individual intensity parameters for each hfs component. In some cases, for the weakest hfs components of these

Table 1. Nb I lines investigated by means of laser optogalvanic spectroscopy (LOGS) or laser-induced fluorescence spectroscopy (LIFS).

λ_{air} (nm)	σ_{vac} (cm^{-1})	Int.	Comment	E_l (cm^{-1})	J_l	E_u (cm^{-1})	J_u	Method, λ_f (nm)
861.445	11 605.22	20		16 828.52	9/2	28 433.74	9/2	LIFS, 527.94
854.725	11 696.46	20		8 410.90	1/2	20 107.36	1/2	LOGS
852.696	11 724.29	50		10 922.74	7/2	22 647.03	5/2	LOGS
847.596	11 794.84	15		9 043.14	5/2	20 837.98	5/2	LOGS
845.672	11 821.67	–	nl	19 556.91	9/2	31 378.58	11/2	LIFS, 491.64
843.981	11 845.35	25		12 357.70	9/2	24 203.05	11/2	LIFS, 467.21
842.317	11 868.76	–	nl	19 931.98	5/2	31 800.74	7/2	LOGS
840.627	11 892.62	15	B(Ne)	15 467.08	5/2	27 359.70	5/2	LIFS, 535.90
839.231	11 912.40	–	nl	20 060.84	7/2	31 973.24	7/2	LIFS, 605.67
835.003	11 972.72	20		8 410.90	1/2	20 383.62	3/2	LOGS
834.601	11 978.48	60		11 044.08	9/2	23 022.56	7/2	LIFS, 539.43
833.743	11 990.81	–	nl	19 034.71	7/2	31 025.52	7/2	LOGS
833.284	11 997.42	–	nl	14 899.26	5/2	26 896.68	7/2	LIFS, 559.95
829.365	12 054.10	3	B(Ne)	13 145.71	9/2	25 199.81	9/2	LIFS, 407.97
827.769	12 077.35	–	nl, B(Nb)	15 282.35	7/2	27 359.70	5/2	LIFS, 535.90
827.490	12 081.42	–	nl	19 931.98	5/2	32 013.40	5/2	LOGS
826.231	12 099.82	4		10 922.74	7/2	23 022.56	7/2	LOGS
823.682	12 137.27	3		15 282.35	7/2	27 419.62	9/2	LOGS
822.609	12 153.10	3	nc B(?)	20 060.84	7/2	32 213.94	9/2	LIFS, 436.84
821.125	12 175.06	3	nc	14 211.30	3/2	26 386.36	5/2	LIFS, 474.06
819.065	12 205.69	4		15 460.77	1/2	27 666.46	1/2	LOGS
818.103	12 220.04	–	nl	22 936.90	7/2	35 156.94	9/2	LIFS, 434.28
817.623	12 227.21	5		15 439.25	3/2	27 666.46	1/2	LOGS
816.847	12 238.83	3	nc	19 568.72	5/2	31 807.55	5/2	LOGS
813.519	12 288.89	80		11 247.88	11/2	23 536.77	9/2	LIFS, 444.58
811.682	12 316.71	–	nl	19 931.98	5/2	32 248.69	3/2	LIFS, 424.63
810.783	12 330.36	2		15 467.08	5/2	27 797.44	5/2	LIFS, 526.99
810.528	12 334.28	–	nl	23 010.58	9/2	35 344.86	11/2	LIFS, 434.90
808.515	12 364.96	4	nc	19 568.72	5/2	31 933.68	5/2	LOGS
803.773	12 437.91	4		13 629.15	1/2	26 067.06	3/2	LOGS
803.606	12 440.49	5	nc	20 060.84	7/2	32 501.33	7/2	LIFS, 490.08
802.878	12 451.77	10		15 467.08	5/2	27 918.85	3/2	LOGS
802.471	12 458.08	4		15 460.77	1/2	27 918.85	3/2	LOGS
801.766	12 469.04	5		9 043.14	5/2	21 512.18	7/2	LIFS, 473.34
801.087	12 479.60	3		15 439.25	3/2	27 918.85	3/2	LOGS
800.755	12 484.78	3		12 288.25	3/2	24 773.03	5/2	LOGS
800.248	12 492.69	8		11 044.08	9/2	23 536.77	9/2	LOGS
798.005	12 527.81	4		14 899.26	5/2	27 427.07	7/2	LOGS
794.565	12 582.04	–	nl	23 048.58	11/2	35 630.62	11/2	LIFS, 414.72
792.281	12 618.32	3		15 460.77	1/2	28 079.09	3/2	LOGS
790.932	12 639.84	3		15 439.25	3/2	28 079.09	3/2	LOGS
790.209	12 651.40	4		10 922.74	7/2	23 574.14	5/2	LOGS
789.857	12 657.03	10	nc	19 556.91	9/2	32 213.94	9/2	LOGS
788.526	12 678.40	60		11 524.65	13/2	24 203.05	11/2	LOGS
788.429	12 679.97	–	nl	19 568.72	5/2	32 248.69	3/2	LIFS, 424.63
787.741	12 691.04	–	nl	19 931.98	5/2	32 623.02	3/2	LIFS, 485.19
787.341	12 697.48	50		14 899.26	5/2	27 596.74	7/2	LOGS
786.266	12 714.84	10	B(Nb)	14 899.26	5/2	27 614.10	5/2	LIFS, 532.15
786.255	12 715.03	–	nl, B(Nb)	17 476.22	11/2	30 191.25	13/2	LIFS, 581.94
785.793	12 722.50	–	nl	19 931.98	5/2	32 654.48	5/2	LIFS, 430.63
785.604	12 725.56	15	B(Ne)	14 211.30	3/2	26 936.86	3/2	LIFS, 539.63
782.696	12 772.84	–	nl	19 034.71	7/2	31 807.55	5/2	LIFS, 610.76
778.709	12 838.24	10	nc	20 060.84	7/2	32 899.08	7/2	LIFS, 410.96
777.208	12 863.03	5	nc	20 060.84	7/2	32 923.87	9/2	LIFS, 480.94
775.090	12 898.18	10		14 899.26	5/2	27 797.44	5/2	LOGS

Notes. E_l, J_l, E_u and J_u are the energy and total electronic angular momentum quantum number of the lower and upper level, respectively; intensities Int. according to Humphreys & Meggers (1945), energy levels according to Humphreys & Meggers (1945) and Kröger et al. (2004, 2007); in the last column the fluorescence wavelength λ_f in air is given for the LIFS measurements; nl: new line; nc: new classification; B(Ne): a neon line, B(Nb) blend by a niobium line, B(?): blend by unclassified line.

Table 1. continued.

λ_{air} (nm)	σ_{vac} (cm^{-1})	Int.	Comment	E_l (cm^{-1})	J_l	E_u (cm^{-1})	J_u	Method, λ_f (nm)
773.586	12 923.25	6		13 629.15	1/2	26 552.40	1/2	LIFS, 578.70
773.026	12 932.61	3	nc B(Ne)	19 568.72	5/2	32 501.33	7/2	LIFS, 490.08
772.673	12 938.53	–	nl, B(Nb)	19 034.71	7/2	31 973.24	7/2	LIFS, 605.67
772.403	12 943.05	3	nc	20 060.84	7/2	33 003.89	7/2	LOGS
771.680	12 955.17	4		11 247.88	11/2	24 203.05	11/2	LIFS, 467.21
770.737	12 971.03	5		11 044.08	9/2	24 015.11	7/2	LOGS
770.308	12 978.25	–	nl	15 467.08	5/2	28 445.33	5/2	LIFS, 444.71
768.660	13 006.08	3		15 439.25	3/2	28 445.33	5/2	LIFS, 527.62
767.833	13 020.08	4		13 145.71	9/2	26 165.79	7/2	LIFS, 583.86
766.276	13 046.54	10	nc	18 332.04	11/2	31 378.58	11/2	LOGS
766.162	13 048.48	10	nc	19 556.91	9/2	32 605.39	9/2	LOGS
765.904	13 052.87	12	nc	19 034.71	7/2	32 087.58	7/2	LOGS
764.179	13 082.34	1		15 467.08	5/2	28 549.42	5/2	LIFS, 429.96
763.979	13 085.76	12	nc	19 568.72	5/2	32 654.48	5/2	LOGS
763.815	13 088.58	15		13 629.15	1/2	26 717.73	1/2	LOGS
762.557	13 110.17	4		15 439.25	3/2	28 549.42	5/2	LOGS
762.113	13 117.81	8		10 126.06	1/2	23 243.87	3/2	LIFS, 452.34
758.561	13 179.23	–	nl	19 034.71	7/2	32 213.94	9/2	LIFS, 436.84
758.526	13 179.83	20	B(?)	14 899.26	5/2	28 079.09	3/2	LIFS, 438.84
758.320	13 183.41	20		12 982.38	7/2	26 165.79	7/2	LIFS, 583.86
754.338	13 253.01	4		15 282.35	7/2	28 535.36	7/2	LIFS, 442.94
754.017	13 258.65	4		11 247.88	11/2	24 506.53	9/2	LIFS, 460.68
753.538	13 267.07	10		15 282.35	7/2	28 549.42	5/2	LIFS, 429.96
751.977	13 294.62	50		13 145.71	9/2	26 440.33	9/2	LIFS, 590.05
751.759	13 298.47	4	nc	19 034.71	7/2	32 333.18	7/2	LOGS
751.237	13 307.71	15		13 629.15	1/2	26 936.86	3/2	LOGS

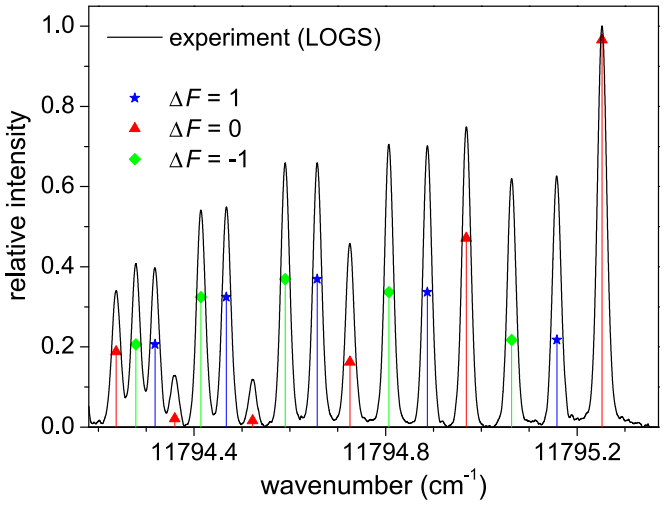

Fig. 3. Fully resolved line to illustrate the magnitude of intensity increase of the weak components. Theoretical relative intensities calculated following Eq. (3) are given as arrows; the arrows are normalised to the strongest hfs component: transition from 9 043.14 cm^{-1}, $J = 5/2 \longrightarrow 20\,837.98$ cm^{-1}, $J = 5/2$ at $\lambda_{air} = 847.596$ nm or $\sigma_{vac} = 11\,794.84$ cm^{-1}.

lines, the fit leads to unreliable values of the Lorentz half width. Then, these parameters were coupled to the same parameter of an other hfs component with the same ΔF.

To analyse the spectra that showed only partly resolved hfs, the number of parameters had to be reduced. This was made in different gradings, as described in the following. Due to the dependence of the saturation effect from the intensity of the hfs components, it made sense to couple profile parameters of hfs components with the same ΔF value, because their intensities are similar in size.

As a first measure, for lines with a partly resolved hfs (as for example shown in Fig. 4a) the parameter for the Lorentzian width were coupled to the same value for each group of hfs components with same ΔF.

If this was not sufficient, depending on the degree of resolution, in some cases the parameter for the Lorentzian width were coupled to the same value for all hfs components and the intensity parameters were additionally coupled for one or more groups of hfs components with the same ΔF according to the theoretical ratios. An example for such a line is given in Fig. 4b.

Some lines look as if they are completely resolved, although this is not the case and most peaks include two or three hfs components. This occurred when one of the involved levels had a very low A constant (i.e. lower than 50 MHz with FWHM of about 600 MHz). For example, the lowest curve in Fig. 2 exhibits this behaviour. To highlight the hfs components, this line is shown again in Fig. 4c together with the fit results.

To analyse spectra with almost unresolved hfs, the number of parameters had to be reduced even more. For this purpose, in addition to all couplings discussed above, the hfs constants A and B of one level were fixed when they were previously known from the literature. An example for such a line is given in Fig. 4d. A list of the hfs constants from the literature and from this work that were fixed during a fit is given in Table 2.

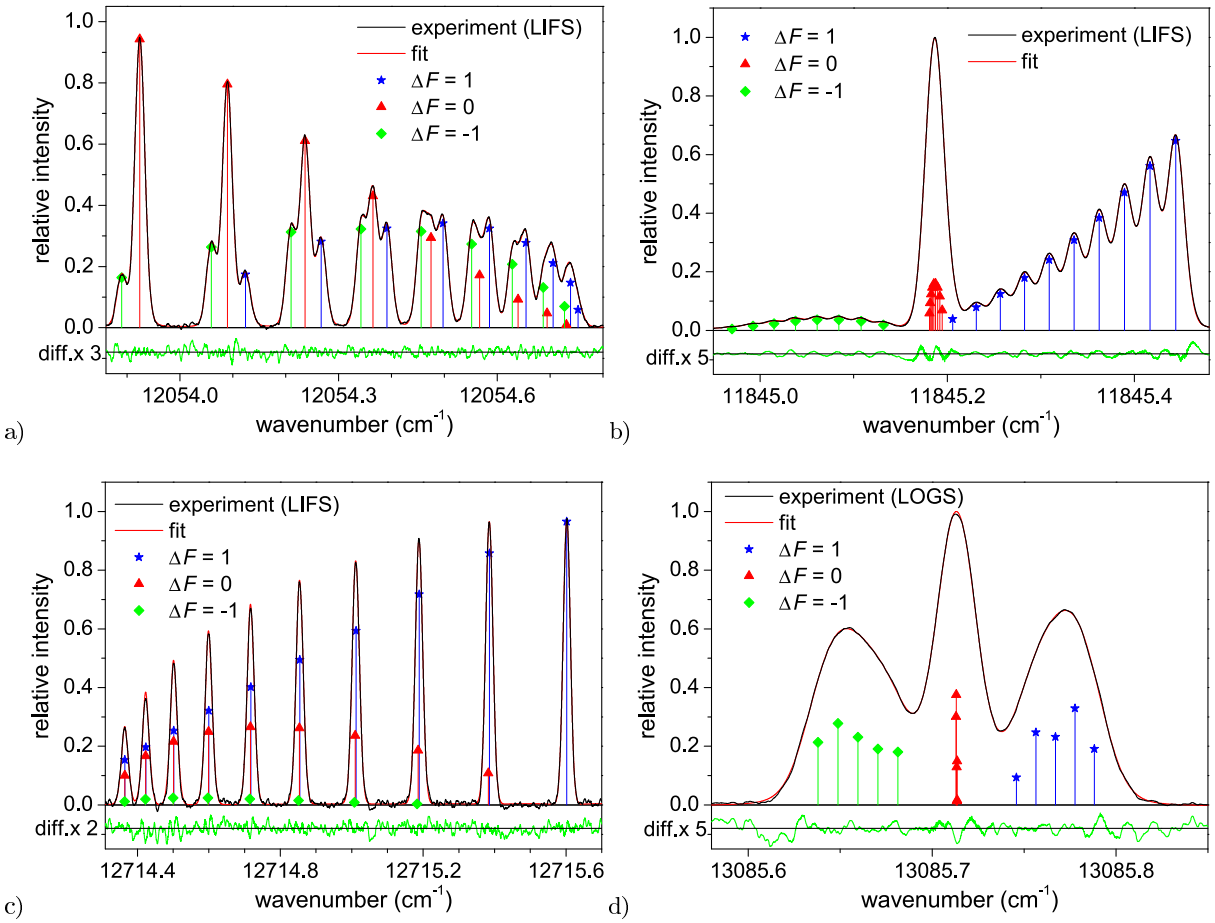

Fig. 4. Hyperfine spectra of the Nb I lines measured with LIFS or LOGS together with the best fitted curve. The hyperfine components are marked by the difference ΔF of the total angular momenta of the lower and upper hyperfine levels. In the lower part of the each figure the residuals between experimental and best fitted curves are given, multiplied by the factor indicated at left side of the graphs. **a)** Example for a line with a rather well resolved hfs, fitted with coupled parameters for the Lorentzian width for each group of hfs components with same ΔF: transition from 13 145.71 cm^{-1}, $J = 9/2 \longrightarrow$ 25 199.81 cm^{-1}, $J = 9/2$ at λ_{air} = 829.365 nm or σ_{vac} = 12 054.10 cm^{-1}. **b)** Example for a partly resolved line, fitted with same parameter for the Lorentzian width for all hfs components and coupled intensity parameters for all hfs components with $\Delta F = 0$: transition from 12 357.70 cm^{-1}, $J = 9/2 \longrightarrow$ 24 203.05 cm^{-1}, $J = 11/2$ at λ_{air} = 843.981 nm or σ_{vac} = 11 845.35 cm^{-1}. **c)** Example for a line that looks like completely resolved, but most peaks include two or three hfs components: transition from 17 476.22 cm^{-1}, $J = 11/2 \longrightarrow$ 30 191.25 cm^{-1}, $J = 13/2$ at λ_{air} = 786.255 nm or σ_{vac} = 12 715.03 cm^{-1}. **d)** Example for an unresolved line fitted with coupled profile parameters, B constants fixed to zero and fixed A constant of the lower level: transition from 19 568.72 cm^{-1}, $J = 5/2 \longrightarrow$ 32 654.48 cm^{-1}, $J = 5/2$ at λ_{air} = 763.979 nm or σ_{vac} = 13 085.76 cm^{-1}.

Table 2. Hyperfine structure constants A and B from the literature and from this work, which were fixed during a fit.

E (cm^{-1})	Config., Term	J	Method	A (MHz)	B (MHz)	Ref.
even parity						
10 126.06	$4d^3(^2P)5s^2\ ^2P$	1/2	LRF	323.6590 (4)	0	(1)
11 247.88	$4d^4(^3H)5s\ ^4H$	11/2	FTS	592 (3)	–	(2)
14 211.30	$4d^4(^3P)5s\ ^4P$	3/2	LIFS	1414.5 (2)	31 (4)	(3)
14 899.26	$4d^4(^3P)5s\ ^4P$	5/2	LIFS	1017.6 (1.4)	7 (4)	t.w.
19 034.71	$4d^4(^3G)5s\ ^2G$	7/2	LIFS	477.6 (8)	57 (40)	t.w.
19 568.72	$4d^4(^1F)5s\ ^2F$	5/2	LIFS	322.4 (4)	–	t.w.
odd parity						
24 015.11	$4d^3(^4F)5s(^5F)5p\ ^4F$	7/2	SAS	591.8 (3)	108 (17)	(4)
24 506.53	$4d^3(^4F)5s(^5F)5p\ ^4F$	9/2	SAS	593.0 (4)	148 (37)	(4)
26 936.86	$4d^4(^5D)5p\ ^6D$	3/2	FTS	39.9 (6)	–	(5)
30 191.25	$4d^3(^2H)5s(^3H)5p\ ^4H$	13/2	FTS	598.8 (5.3)	–	(2)
31 378.58	$4d^3(^2G)5s(^1G)5p\ ^2H$	11/2	LIFS	791.1 (1.2)	−236 (50)	t.w.
35 344.86	$4d^4(^3H)5p\ ^4I$	11/2	FTS	510.0 (3.1)	–	(5)

Notes. LRF – laser radio-frequency double resonance, FTS – Fourier transform spectroscopy, LIFS – laser-induced fluorescence spectroscopy, SAS – saturation absorption spectroscopy.

References. t.w.: this work; (1) Fraenkel et al. (1988); (2) Er et al. (2011); (3) Bouzed et al. (2003); (4) Başar et al. (2008); (5) Kröger et al. (2010).

Table 3. Experimental hyperfine structure constants A_{exp} and B_{exp} (in MHz) of the levels of even parity of Nb I together with comparative values A_{ref} and B_{ref}, if available.

E (cm^{-1})	Config., Term	J	λ_{air} (nm)	A_{exp} (MHz)	A_{mean} (MHz)	B_{exp} (MHz)	B_{mean} (MHz)	A_{ref} (MHz)	B_{ref} (MHz)	Ref.
8410.90	4d^4(^{5}D)5s ^{4}D	1/2	854.725	1996.7 (2)	1996.7 (1)	0	0	1996(1)	0	(1)
			835.003	1995.8 (1.6)		0				
9043.14	4d^4(^{5}D)5s ^{4}D	5/2	847.596	–407.6 (2)	–407.59 (3)	41 (8)	38 (3)	–407.8606(43)	35.060(75)	(2)
			801.766	–407.5 (6)		35 (8)				
10 922.74	4d^4(^{3}H)5s ^{4}H	7/2	852.696	–157.7 (1.2)	–159.5 (6)	–	–46.4 (9)	–169(9)	–	(3)
			826.231	–159.9 (6)		–45 (34)				
			790.209	–160.4 (2.0)		–47 (22)				
11 044.08	4d^4(^{3}H)5s ^{4}H	9/2	834.601	372 (5)	373.1 (4)	–		372.9(7)	–	(3)
			800.248	372.7 (6)		–				
			770.737*	373.8 (8)		–				
11 247.88	4d^4(^{3}H)5s ^{4}H	11/2	771.680	593.8 (1.2)	593.9 (1)	–		592(3)	–	(3)
			754.017*	594.0 (0.6)		–				
11 524.65	4d^4(^{3}H)5s ^{4}H	13/2	788.526	704.9 (2.8)		–		700(4)	–	(3)
12 288.25	4d^4(^{3}F)5s ^{4}F	3/2	800.755	–592.2 (2.8)		35 (24)		–592(2)	–	(1)
12 357.70	4d^4(^{3}F)5s ^{4}F	9/2	843.981	739.7 (1.0)		10 (50)		740(2)	–	(1)
12 982.38	4d^4(^{3}G)5s ^{4}G	7/2	758.320	568.2 (4)		–		563.9(2)	–	(3)
13 145.71	4d^4(^{3}G)5s ^{4}G	9/2	829.365	663.3 (6)	663.1 (4)	55 (30)	69.0 (4)	667(5)	–	(4)
			767.833	662.3 (1.0)		74 (18)				
			751.977	666 (4)		–				
13 629.15	4d^3(^{4}P)5s^2 ^{4}P	1/2	803.773	2938 (3)	2938.8 (6)	0	0	2939.1(8)	0	(5)
			773.586	2938.7 (1.8)		0				
			763.815	2939 (3)		0				
			751.237*	2945 (9)		0				
14 211.30	4d^4(^{3}P)5s ^{4}P	3/2	821.125	1417.4 (1.6)		15 (24)		1414.5(2)	31(4)	(5)
14 899.26	4d^4(^{3}P)5s ^{4}P	5/2	798.005	1016.0 (8)	1017.6 (6)	8 (24)	7 (2)	–	–	
			787.341	1018.9 (6)		4 (32)				
			786.266	1017.2 (2.0)		–				
			775.090	1016.6 (1.0)		–				
			758.526	1016.9 (1.6)		–				
15 282.35	4d^4(^{3}D)5s ^{4}D	7/2	827.769	982 (8)	981.5 (1)	–	–22 (3)	988(5)	–	(1)
			823.682	981.6 (1.0)		–24 (18)				
			754.338	981.2 (1.2)		–				
			753.538	981.6 (1.2)		–17 (26)				
15 439.25	4d^4(^{3}D)5s ^{4}D	3/2	817.623	481.5 (8)	481.6 (2)	105 (4)	106 (1)	–	–	
			801.087	482 (3)		111 (24)				
			790.932	482.2 (2.2)		102 (22)				
			768.660	480 (3)		116 (30)				
			762.557	481.9 (1.2)		110 (14)				
15 460.77	4d^4(^{3}D)5s ^{4}D	1/2	819.065	–1134.7 (2.0)	–1135.8 (1.3)	0	0	–	–	
			802.471	–1140 (4)		0				
			792.281	–1135 (4)		0				
15 467.08	4d^4(^{3}D)5s ^{4}D	5/2	840.627	833.4 (2.8)	833.4 (5)	–143 (36)	–120 (5)	–	–	
			810.783	831.8 (1.2)		–104 (28)				
			802.878	833.1 (1.6)		–117 (16)				
			770.308	834.5 (8)		–123 (24)				
			764.179	832.7 (1.2)		–124 (56)				
16 828.52	4d^4(^{1}G)5s ^{2}G	9/2	861.445	744.4 (6)		57 (12)		743.6 (1.2)	–	(1)
17 476.22	4d^4(^{1}I)5s ^{2}I	11/2	786.255*	11 (8)		–		–20 (19)	–	(3)
18 332.04	4d^4(^{3}H)5s ^{2}H	11/2	766.276*	2.9 (6)		–94 (44)		–	–	
19 034.71	4d^4(^{3}G)5s ^{2}G	7/2	833.743	478.3 (1.4)	477.6(4)	–		–	–	
			772.673	475.9 (1.0)		57 (40)				

Notes. Configurations and terms according to Kröger & Bouzed (2003); the wavelength given in the fifth column specifies the line that was used to determine the A_{exp} and B_{exp} values; when a hyperfine structure constant was determined by more than one line, the weighted mean value A_{mean} and B_{mean}, respectively, are given, calculated by using the error bar of A_{exp} and B_{exp} as weight. In columns A_{mean} and B_{mean}, twice the standard deviation that resulted from the weighted mean value calculation is given as error. (*) Hyperfine structure constants of upper level were fixed during the fit.

References. (1) Başar et al. (2008); (2) Fraenkel et al. (1988); (3) Er et al. (2011); (4) Kröger (2007); (5) Bouzed et al. (2003).

Table 3. continued.

E (cm^{-1})	Config., Term	J	λ_{air} (nm)	A_{exp} (MHz)	A_{mean} (MHz)	B_{exp} (MHz)	B_{mean} (MHz)	A_{ref} (MHz)	B_{ref} (MHz)	Ref.
			765.904	477.4 (8)		–				
			758.561	477.6 (4)		–				
			751.759	482.2 (1.6)		–				
19 556.91	$4d^4(^3G)5s\ ^2G$	9/2	845.672	112.8 (6)	112.7 (1)	17 (12)	–12 (25)	–	–	
			789.857	112.3 (1.2)		–33 (10)				
			766.161	112.6 (1.6)		–				
19 568.72	$4d^4(^1F)5s\ ^2F$	5/2	808.515	322.4 (1.0)	322.4 (2)	–		–	–	
			788.429	322.6 (1.4)		–				
			773.026	319.8 (1.4)		–				
19 931.98	$4d^4(^3D)5s\ ^2D$	5/2	842.317	531 (11)	529.0 (6)	–		–	–	
			827.490	528 (14)		–				
			811.682	529 (5)		–				
			787.741	529.9 (1.8)		–				
			785.793	527.5 (2.2)		–				
20 060.84	$4d^4(^3F)5s\ ^2F$	7/2	839.231	242.5 (2.4)	244.5 (3)	23 (24)	2 (3)	–	–	
			822.609	242.3 (1.2)		13 (22)				
			803.606	244.6 (2)		1 (4)				
			778.709	238 (4)		–				
			777.208	242.9 (2.2)		–				
			772.403	242.1 (1.4)		11 (80)				
22 936.90	$4d^5\ ^4G$	7/2	818.103	266 (5)		–		–	–	
23 010.58	$4d^5\ ^4G$	9/2	810.526*	94 (10)		–		–	–	
23 048.58	$4d^5\ ^4G$	11/2	794.565	82 (4)		–		–	–	

5. Results and discussion

Altogether, 81 spectral lines were investigated by laser excitation i.e LOGS and LIFS. They are listed in Table 1 along with their wavelengths in air λ_{air}, wave numbers in vacuum σ_{vac}, intensities and classifications. In the last column of Table 1, the experimental method used, LOGS or LIFS, is specified. When LIFS was used, the corresponding fluorescence wavelength is given in the last column. The wave numbers in vacuum were calculated as energy differences from the upper and lower level: $\sigma_{vac} = E_u - E_l$. The experimental centre of the gravity wave number in vacuum of the lines can be determined by using the start wave number of laser scan and fitting the centre of gravity of the hfs. These experimental values agree within an interval of ±0.02 cm^{-1} with the calculated wave number σ_{vac} given in Table 1. The wavelengths in air were calculated from the wave numbers in vacuum using the dispersion relation (Peck & Reader 1972). The intensities and classifications are given according to Humphreys & Meggers (1945) when a line was listed in this wavelength table. Nineteen lines are new lines, which mean they have not previously been published. They are denoted as "nl". Additionally, 16 lines measured in the present work were given in the wavelength tables of Humphreys & Meggers (1945) without classification. They have newly been classified here and are denoted as "nc". When a line is overlapping within its hfs pattern with another Nb or with a Ne line, this is commented as "B" (blend) in Table 1.

The resulting hfs constants A_{exp} and B_{exp} are listed in Tables 3 and 4 for the levels of even and odd parity, respectively. Level energies are given according to Humphreys & Meggers (1945) and Kröger et al. (2004, 2007), configurations and terms according to Kröger & Bouzed (2003) for levels of even parity and according to Kröger et al. (2007) for levels of odd parity. The wavelength λ_{air} given in the fifth column specifies the line that was used to determine the hfs constants A_{exp} and B_{exp}. All spectra were recorded and fitted five times or more, depending on the signal-to-noise ratio. The given A_{exp} and B_{exp} are the statistic mean value of the fit results of all measurements, the measurement uncertainty being twice the corresponding standard. These errors refer only to the statistical variation of the fit and do not include systematic errors, which may occur because of the coupling of profile or intensity parameters during the fit. Hence the measurement uncertainty may be higher than the given statistical error bar. This fact can be exemplified by some hfs constants A_{exp} or B_{exp}, determined from different lines, which do not agree with each other within the limits of given errors. Nevertheless, the statistical errors convey an idea of the accuracy of the fit value.

When a hfs constant of a level was measured by two or more lines, the weighted mean value A_{mean} and B_{mean} was taken, using the error limits of A_{exp} and B_{exp} as weight. The measurement uncertainties given for the mean values A_{mean} are twice the standard deviations corresponding to this average.

6. Conclusion and outlook

In total, we have determined the magnetic dipole hyperfine structure constants A for 81 energy levels of atomic Nb and additionally the electric quadrupole hyperfine structure constants B for 41 of these levels. For 13 levels of even parity and for 11 levels of odd parity the A constants were measured for the first time. Additionally, the electric quadrupole hfs constants B for 30 levels were measured for the first time. Beyond that, already known A and B constants were verified and in some cases the accuracy was improved.

The present work constitutes another contribution to complete the hfs data of atomic Nb and provides this data for users, especially in astrophysics. Including the new results of the present work, the magnetic dipole hfs constants A are now known for all known energy levels of even parity.

Table 4. Experimental hyperfine structure constants A_{exp} and B_{exp} (in MHz) of the levels of odd parity of Nb I together with comparative values A_{ref} and B_{ref}, if available.

E (cm^{-1})	Config., Term	J	λ_{air} (nm)	A_{exp} (MHz)	A_{mean} (MHz)	B_{exp} (MHz)	B_{mean} (MHz)	A_{ref} (MHz)	B_{ref} (MHz)	Ref.
20 107.36	4d^3(^{4}F)5s(^{5}F)5p ^{4}D	1/2	854.725	–794.1 (2.6)		0		–794.7 (5)	0	(6)
20 383.62	4d^3(^{4}F)5s(^{5}F)5p ^{4}D	3/2	835.003	597.4 (4)		–14 (6)		597.8 (5)	–13 (4)	(1)
20 837.98	4d^3(^{4}F)5s(^{5}F)5p ^{4}D	5/2	847.596	808.6 (6)		–15 (14)		808.8 (4)	–14 (6)	(1)
21 512.18	4d^3(^{4}F)5s(^{5}F)5p ^{4}D	7/2	801.766	871.9 (6)		–24 (16)		872.8 (5)	–27 (6)	(1)
22 647.03	4d^3(^{4}F)5s(^{5}F)5p ^{4}G	5/2	852.696	–74.3 (1.4)		–		–78.5 (2)	–	(6)
23 022.56	4d^3(^{4}F)5s(^{5}F)5p ^{4}G	7/2	826.231 834.601	430.1 (6) 424 (7)	430.1 (5)	1 (16) –		430.3 (2)	–	(6)
23 243.87	4d^3(^{4}F)5s(^{5}F)5p ^{4}F	3/2	762.113*	–14.4 (6)		–		–16.6 (3)	–	(6)
23 536.77	4d^3(^{4}F)5s(^{5}F)5p ^{4}G	9/2	800.248 813.519*	629.9 (1.0) 629 (4)	629.9 (2)	– –		632.6 (1)	–	(6)
23 574.14	4d^3(^{4}F)5s(^{5}F)5p ^{4}F	5/2	790.209	512 (4)		102 (26)		514.1 (2)	67 (5)	(1)
24 203.05	4d^3(^{4}F)5s(^{5}F)5p ^{4}G	11/2	771.680 788.526 843.981	751.3 (1.0) 754.3 (2.2) 748.8 (8)	750.1 (1.2)	– – 0 (60)		752.3 (1)	–	(6)
24 773.03	4d^3(^{4}F)5s(^{3}F)5p ^{2}D	5/2	800.755	170.5 (1.2)		17 (40)		170.1 (5)	–11 (7)	(1)
25 199.81	4d^4(^{5}D)5p ^{6}F	9/2	829.365	113.1 (4)		33 (32)		112.4 (4)	–	(6)
26 067.06	4d^3(^{4}P)5s(^{5}P)5p ^{6}D	3/2	803.773	938.9 (1.2)		49 (32)		943.5 (1.8)	79 (3)	(5)
26 165.79	4d^4(^{5}D)5p ^{6}F	7/2	758.320 767.833	299.1 (4) 294.9 (1.2)	298.7 (1.3)	– 65 (20)		297.6 (7)	–	(6)
26 386.36	4d^3(^{4}P)5s(^{5}P)5p ^{6}D	5/2	821.125	810.9 (1.0)		64 (68)		809.2 (5)	64.2 (9.3)	(2)
26 440.33	4d^4(^{5}D)5p ^{4}F	9/2	751.977	342 (8)		–		337.6 (2)	88.6 (8.1)	(2)
26 552.40	4d^4(^{5}D)5p ^{6}D	1/2	773.586	430.3 (1.8)		0		430.1 (5)	0	(2)
26 717.73	4d^3(^{4}F)5s(^{3}F)5p ^{4}D	1/2	763.815	507.0 (2.8)		0		508.3 (4)	0	(2)
26 896.68	4d^3(^{2}G)5s(^{3}G)5p ^{4}H	7/2	833.284*	181.3 (2.8)		–21 (40)		–	–	
26 936.86	4d^4(^{5}D)5p ^{6}D	3/2	785.604*	39.9 (1.6)		–		39.9 (6)	–	(6)
27 359.70	4d^4(^{5}D)5p ^{4}D	5/2	827.769 840.627	–20 (10) –20 (3)	–20 (0)	– 11 (32)		–22.4 (1.2)	–	(6)
27 419.62	4d^3(^{4}P)5s(^{5}P)5p ^{6}D	9/2	823.682	405.7 (8)		47 (16)		405.4 (9)	94 (20)	(5)
27 427.07	4d^4(^{5}D)5p ^{6}D	7/2	798.005	385.8 (4)		–52 (32)		386.0 (5)	–38.2 (15.2)	(2)
27 596.74	4d^4(^{5}D)5p ^{4}D	7/2	787.341	–149.3 (8)		60 (20)		–151.4 (7)	–	(3)
27 614.10	4d^3(^{2}P)5s(^{3}P)5p ^{4}P	5/2	786.266	616.2 (1.6)		–		615 (2)	–	(1)
27 666.46	4d^3(^{2}P)5s(^{3}P)5p ^{4}D	1/2	817.623 819.065	725.5 (1.6) 726.2 (1.0)	726.0 (3)	0 0		729.7 (2.3)	0	(6)
27 797.44	4d^3(^{4}F)5s(^{3}F)5p ^{2}F	5/2	775.090 810.783	569.0 (6) 567.4 (8)	568.4 (8)	– 24 (14)		568.4 (4.9)	–	(6)
27 918.85	4d^4(^{5}D)5p ^{4}D	3/2	801.087 802.471 802.878	344.7 (2.4) 343.7 (1.4) 344.4 (1.4)	344.2 (3)	–33 (12) –24 (16) –35 (6)	–33.5 (2.3)	348 (1)	–	(6)
28 079.09	4d^3(^{4}P)5s(^{5}P)5p ^{4}P	3/2	758.526 790.932 792.281	677.8 (1.6) 676.8 (2.2) 676.1 (1.2)	676.8 (5)	–36 (24) –34 (8) –36 (10)	–34.9 (7)	676.2 (3)	–	(6)
28 433.74	4d^3(^{4}F)5s(^{3}F)5p ^{2}G	9/2	861.445	178.5 (6)		–60 (6)		179.5 (4)	–48 (12)	(1)
28 445.33	4d^3(^{4}P)5s(^{5}P)5p ^{4}P	5/2	770.308 768.660	617.0 (1.0) 613.9 (2.0)	616.4 (1.2)	–75 (20) –47 (46)	–70 (10)	614 (1)	–	(6)
28 535.36	4d^3(^{2}P)5s(^{3}P)5p ^{4}D	7/2	754.338	659.2 (1.0)		–		660.5 (9)	–	(6)
28 549.42	4d^3(^{4}P)5s(^{5}P)5p ^{4}P	5/2	753.538 762.557	676.7 (1.0) 677.3 (6)	677.0 (3)	–13 (22) 1 (28)	–9 (5)	676.9 (9)	–	(6)

Notes. Configurations and terms according to Kröger et al. (2007); the wavelength given in the fifth column specifies the line that was used to determine the A_{exp} and B_{exp} values; when a hyperfine structure constant was determined by more than one line, the weighted mean value A_{mean} and A_{mean}, respectively, are calculated, using error bar of A_{exp} and B_{exp} as weight. In column A_{mean}, twice the standard deviation that resulted from the weighted mean value calculation is given as error. (*) Hyperfine structure constants of lower level were fixed during the fit.

References. (1) Başar et al. (2008); (2) Fraenkel et al. (1988); (3) Er et al. (2011); (4) Kröger (2007); (5) Bouzed et al. (2003); (6) Kröger et al. (2010).

Table 4. continued.

E (cm^{-1})	Config., Term	J	λ_{air} (nm)	A_{exp} (MHz)	A_{mean} (MHz)	B_{exp} (MHz)	B_{mean} (MHz)	A_{ref} (MHz)	B_{ref} (MHz)	Ref.
			764.179	676.1 (1.6)		–22 (70)				
31 025.52	$4d^3(^4F)5s(^3F)5p\ ^2F$	7/2	833.743	361.7 (1.2)		–		–	–	
31 378.58	$4d^3(^2G)5s(^1G)5p\ ^2H$	11/2	845.672	791.1 (1.2)		–236 (50)		–	–	
31 800.74	$4d^3(^2G)5s(^3G)5p\ ^2G$	7/2	842.317	220 (7)		–		217.4 (9)	–	(6)
31 807.55	$4d^3(^2D_2)5s(^3D)5p\ ^4D$	5/2	816.847*	450 (8)	451.9 (1.4)	–		–	–	
			782.696*	453 (6)		–				
31 933.68	$4d^3(^4F)5s(^3F)5p\ ^4G$	5/2	808.515	567.5 (1.4)		–		–	–	
31 973.24	$4d^3(^2D_2)5s(^3D)5p\ ^4D$	7/2	772.673	742.5 (1.0)	742.6 (1)	56 (44)	53 (3)	–	–	
			839.231	742.9 (2.4)		50 (40)				
32 013.40	$4d^3(^2D_2)5s(^3D)5p\ ^4F$	5/2	827.490	538 (14)		–		–	–	
32 087.58	$4d^4(^3H)5p\ ^2G$	7/2	765.904	317.7 (8)		–		316 (2)	–	(1)
32 213.94	$4d^3(^2H)5s(^3H)5p\ ^4I$	9/2	758.561	594.7 (4)	594.6 (2)	–	–1 (22)	594.8 (1.5)	–	(6)
			789.857	594.5 (1.8)		–14 (32)				
			822.609	593.2 (2.0)		35 (52)				
32 248.69	$4d^3(^4P)5s(^5P)5p\ ^4D$	3/2	811.682	594 (6)	593.6 (2)	–		–	–	
			788.429	593.5 (2.6)		–				
32 333.18	$4d^3(^2D_2)5s(^3D)5p\ ^4F$	7/2	751.759	451.3 (1.2)		–		451.3 (4.4)	–	(6)
32 501.33	$4d^4(^3H)5p\ ^2G$	7/2	803.606	593.8 (1.2)	592.2 (1.4)	–25 (14)		589.7 (1.7)	–	(3)
			773.026	591.0 (1.0)		–				
32 605.39	$4d^4(^3H)5p\ ^2G$	9/2	766.161	272.5 (1.6)		–		270.5 (1)	–	(6)
32 623.02	$4d^3(^4P)5s(^3P)5p\ ^2P$	3/2	787.741	499.5 (2.2)		–		–	–	
32 654.48	$4d^3(^4F)5s(^3F)5p\ ^4F$	5/2	763.979*	330 (14)	318.5 (1.5)	–		321 (11)	–	(6)
			785.793	318.3 (1.8)		–				
32 899.08	$4d^3(^4F)5s(^3F)5p\ ^4F$	7/2	778.709	203 (5)		–		218.4 (12.1)	–	(6)
32 923.87	$4d^3(^2D_2)5s(^3D)5p\ ^4F$	9/2	777.208	667.4 (1.6)		–110 (100)		668.9 (3.1)	–	(3)
33 003.89	$4d^3(^4P)5s(^5P)5p\ ^4D$	7/2	772.403	441 (4)		–		–	–	
35 156.94	$4d^3(^2H)5s(^3H)5p\ ^4G$	9/2	818.103	517 (5)		–		510.0 (3.1)	–	(6)
35 630.62	$4d^3(^2H)5s(^3H)5p\ ^4G$	11/2	794.565	548 (4)		–		–	–	

Based on these data, it is highly recommended that an improved theoretical analysis for levels of even and odd parity is undertaken. Additionally, the search for new fine structure energy levels should proceed. From an atomic physical point of view, it would be of great interest to measure the hfs constants, especially the electric quadrupole constants B, with higher accuracy using Doppler-free experimental methods.

Acknowledgements. Gö. Başar thanks for the research fund of the Istanbul University Scientific Research Projects with project number No. 6222. I. K. Öztürk thanks for the research fund of the Istanbul University Scientific Research Projects with project number No. 6221. We thank Ali Sami Gözükırmızı for the data acquisition program.

References

Başar, G., Başar, G., Bayram, B., & Kröger, S. 2008, Phys. Scr., 78, 015303
Bouzed, A., Kröger, S., Zimmermann, D., Kronfeldt, H.-D., & Guthöhrlein, G. 2003, Eur. Phys. J. D, 23, 57
Büttgenbach, S., & Dicke, R. 1975, Z. Phys. D, 275, 197
Büttgenbach, S., Dicke, R., Gebauer, H., Herschel, M., & Meisel, G. 1975, Z. Phys. D, 275, 193
Er, A., Öztürk, I., Başar, G., et al. 2011, J. Phys. B: At. Mol. Opt. Phys., 44
Fraenkel, L., Bengtsson, C., Hanstorp, D., Nyberg, A., & Persson, J. 1988, Z. Phys. D, 8, 171
Guthöhrlein, G. H. 2004, University of Bundeswehr Hamburg, unpublished
Humphreys, C. J., & Meggers, W. F. 1945, J. Res. Nat. Bur. Stand, 34, 478
Kröger, S. 2007, Eur. Phys. J. D, 41, 55
Kröger, S., & Bouzed, A. 2003, Eur. Phys. J. D, 23, 63
Kröger, S., Scharf, O., & Guthöhrlein, G. 2004, Europhys. Lett., 66, 344
Kröger, S., Öztürk, I. K., Acar, F. G., et al. 2007, Eur. Phys. J. D, 41, 61
Kröger, S., Er, A., Öztürk, I. K., et al. 2010, A&A, 516, A1
Lederer, C. M., & Shirley, V. S. 1978, Table of isotopes, 7th edn (New York: Wiley)
Messnarz, D., & Guthöhrlein, G. H. 2000, Eur. Phys. J. D, 12, 269
NIST 2013, NIST Atomic Spectra Database Version 5, Website
Peck, R., & Reader, K. 1972, JOSA, 62
Sasso, A. 1990, Rev. Mod. Phys., 82, 603
Shamim, K., Siddiqui, I., & Windholz, L. 2011, Eur. Phys. J. D, 64
Singh, R., & Rao, G. N. 1989, Phys. Scr., 40, 170
Singh, R., Thareja, R. K., & Rao, G. N. 1992, J. Opt. Soc. Am. B, 9, 493
Windholz, L., & Guthöhrlein, G. H. 2003, Phys. Scr. T, 105, 55